OPEN ACCESS
IOP Publishing | IMMT
International Journal of Extreme Manufacturing
Int. J. Extrem. Manuf. 4 (2022) 035001 (7pp)
https://doi.org/10.1088/2631-7990/ac6cb0

Electro- and photochemical studies of gold (III) bromide towards a novel laser-based method of gold patterning

Cecily Rosenbaum, Matthew Murphy, Paul T Lawrence, Curtis Sirkoch, Stella Rose Schneeberg, Kyle Zigner, Sarah Morris, Ethan Richman, Chibuzo Anyanwu, Eric Will, Clare Wheeler, Eric Reed and Christopher N LaFratta*

Department of Chemistry and Biochemistry, Bard College, Annandale-on-Hudson, NY, United States of America

E-mail: clafratt@bard.edu

Received 23 August 2021, revised 29 October 2021
Accepted for publication 3 May 2022
Published 7 June 2022

Abstract

In this report, we demonstrate a novel technique for the microscopic patterning of gold by combining the photoreduction of $Au^{III}Br_4^-$ to $Au^{I}Br_2^-$ and the electrochemical reduction of $Au^{I}Br_2^-$ to elemental gold in a single step within solution. While mask-based methods have been the norm for electroplating, the adoption of direct laser writing for flexible, real-time patterning has not been widespread. Through irradiation using a 405 nm laser and applying a voltage corresponding to a selective potential window specific to $Au^{I}Br_2^-$, we have shown that we can locally deposit elemental gold at the focal point of the laser. In addition to demonstrating the feasibility of the technique, we have collected data on the kinetics of the photoreduction reaction in ethanol and have deduced its rate law. We have confirmed the selective deposition of $Au^{I}Br_2^-$ within a potential window through controlled potential electrolysis experiments and through direct measurement on a quartz crystal microbalance. Finally, we have verified local deposition through scanning electron microscopy.

Keywords: photolithography, direct laser writing, electrodeposition, gold (III) bromide, photoreduction

1. Introduction

Due to the excellent electrical and electrochemical properties of gold and its use in sensors, actuators, and circuits the development of new lithographic methods for patterning is a continually evolving field of research [1–4]. The primary method for patterning metal follows a two-step process: (a) a patterning step to define where the metal will be placed and (b) a growth step to deposit the metal. These are usually done by photo- or e-beam-lithography, followed by thermal deposition or electroplating. Electroless deposition of coinage metals is also common when depositing onto nonconductive surfaces [5–10]. Alternative methods that use a single step to directly pattern the metal offer distinct advantages over mask-based methods. Many of these single step methods use a focused laser, such as: vapor phase deposition [11], photoreduction of metal-organic frameworks [12] and simultaneous two-photon polymerization and photoreduction [13, 14]. Some of these direct laser writing (DLW) methods rely on a combination of photochemical excitation and thermal excitation to nucleate metal nanoparticles which then grow and join together. One issue with photoreduced metals is that, because of the use of organic reducing agents and the nucleation mechanism

* Author to whom any correspondence should be addressed.

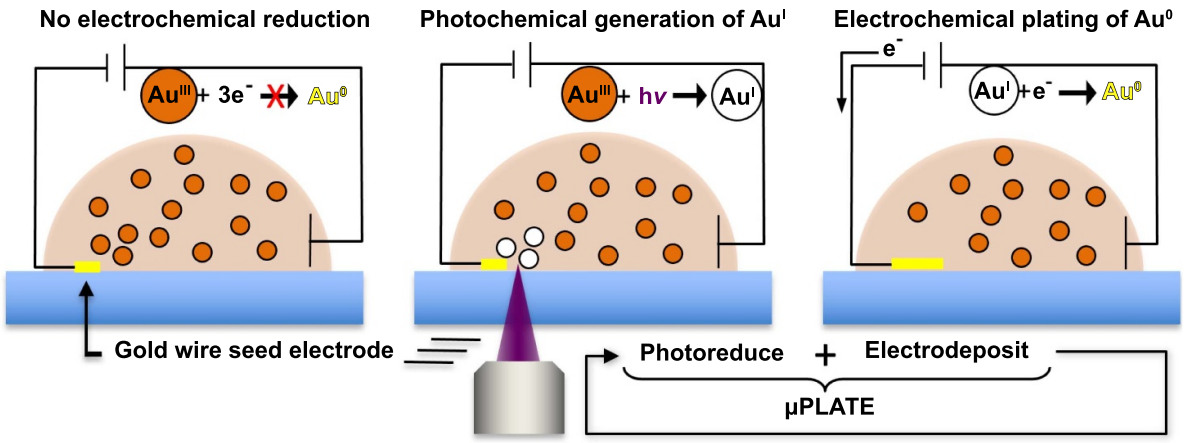

Figure 1. μPLATE process. (Left) A $Au^{III}Br_4^-$ solution with a gold working electrode is at a potential that does not plate $Au^{III}Br_4^-$. (Middle) Irradiation of the solution with a 405 nm laser focused near the electrode causes the reduction of $Au^{III}Br_4^-$ to $Au^{I}Br_2^-$. (Right) Localized electrodeposition of $Au^{I}Br_2^-$ to Au^0 takes place onto the working electrode.

[15], they tend to have lower conductivity than electroplated or vapor deposited patterns [16–21]. While electroplating and vapor deposition produce high-quality metal features, patterns are reliant on pre-fabricated masks and, thus, cannot match the flexibility of DLW. Laser exposure can be coupled to electroplating as a patterning technique and has been demonstrated in several different ways. In one method the laser is used to thermally enhance the patterning [22, 23] while in another the laser is used to remove a protective oxide coating [24]. Au nanoparticles have also been assembled using a combination of electrophoresis and laser trapping to create microstructures [25, 26] as well as laser sintering [27–31]. Gold has also been patterned on graphene using photo-induced electron–hole formation to locally reduce gold from solution [32].

The method described below, which we call: microscale photochemical laser traced electrodeposition, or μPLATE, couples the processes of photoreduction and electroplating into a single patterning step. Briefly, the μPLATE method uses a focused laser to locally convert Au^{III} in solution to Au^{I} and subsequently electroplate the Au^{I} to Au^0. Since the Au^{I} will only be created in the vicinity of the laser exposure, the laser will be able to direct or trace where the electrode will grow. The combination of photo-redox and applied potentials has recently been demonstrated as an effective gold film etching technique [33]. In this work, we seek to prove the potential of μPLATE as an additive technique, which, once optimized, is expected to require a smaller quantity of gold compared to similar subtractive techniques.

Figure 1 illustrates how μPLATE works. A seed electrode is placed in a solution containing $Au^{III}Br_4^-$ and ethanol with a potential applied that is too positive to cause reduction of the $Au^{III}Br_4^-$. A laser is tightly focused through an objective lens into the sample, close in proximity to the gold seed electrode, allowing for the localized photoreduction of $Au^{III}Br_4^-$ to $Au^{I}Br_2^-$. While the $Au^{III}Br_4^-$ absorbs the laser and is photoreduced, the resulting $Au^{I}Br_2^-$ is transparent at 405 nm and cannot undergo further photoreduction to Au^0. The potential of the electrode can selectively reduce $Au^{I}Br_2^-$, thus electroplating Au^0 onto the seed electrode. The standard reduction potentials for $Au^{III}Br_4^-$ and $Au^{I}Br_2^-$ vs SHE are shown below [34].

$$Au^{III}Br_4^- + 3e^- \rightarrow Au^0 + 4Br^- \ (E^\circ + 0.960\ \mathrm{V}) \quad (1)$$

$$Au^{I}Br_2^- + 1e^- \rightarrow Au^0 + 2Br^- \ (E^\circ + 0.858\ \mathrm{V}). \quad (2)$$

These indicate that there should exist a potential window to enable the selective deposition of only $Au^{I}Br_2^-$.

In this work, both the electrochemical and photochemical aspects of the μPLATE method were examined. The kinetics of the photochemical reduction of $Au^{III}Br_4^-$ were studied using a homemade laser photometer system and a rate law was determined. Controlled potential electrolysis (CPE) experiments were used over a range of voltages to identify a potential that enabled the selective deposition of $Au^{I}Br_2^-$ in the presence of $Au^{III}Br_4^-$. Also, the rate of deposition was studied with a quartz crystal microbalance (QCM) as the ratio of $Au^{I}Br_2^-$:$Au^{III}Br_4^-$ changed. Finally, results are shown from a proof of concept experiment where gold was locally deposited via the μPLATE method.

2. Methods and materials

Gold wire, 99.95% pure and 25 μm in diameter, was purchased from Alfa Aesar. The $AuBr_3$, 99.9%, (the precursor of $Au^{III}Br_4^-$ in the presence of Br^-) and all other reagents were used as received from Sigma-Aldrich.

2.1. Photoreduction kinetics

A solution containing 0.10 M $NaClO_4$, 0.10 M HBr, and 0.15 mM $Au^{III}Br_4^-$ was prepared in a solution of ethanol:water::3:1 (v/v). This solution was placed in a 1 cm pathlength cuvette and the absorbance spectra was recorded using a Cary 300 UV–vis spectrophotometer. The instrument was blanked with the same solution excluding the $Au^{III}Br_4^-$. The cuvette was irradiated with a 405 nm laser (Coherent, OBIS)

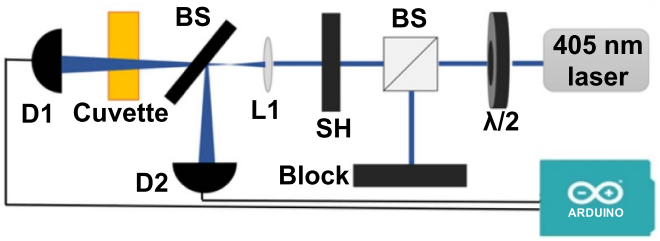

Figure 2. Photometer schematic. From right to left, the laser beam passes through a half-wave plate then through a PBS, a shutter (SH), and is expanded with lens (L1). A second beam splitter (BS) divides the beam. One portion is collected by reference detector, D2, the other passes through a cuvette and the remaining light is collected by detector D1. Data are collected using a customized Arduino system.

with 1.5 mW for 120 min and periodically removed to measure the absorption spectrum.

To determine the rate of the photochemical reduction, a homemade laser photometer was assembled as shown in figure 2. The 405 nm laser was passed through a half-wave plate and a polarizing beam splitter (PBS) to enable the power to be adjusted. Next, the beam was slightly expanded before hitting a 50/50 beam splitter, where a reference detector, D1, (Thorlabs PDA100A) measured any laser fluctuations. The transmitted light completely exposed the 0.1 ml of solution in the cuvette (Thorlabs CV10Q100) before being detected on the second photodiode, D2. The signals from both detectors were measured for 30 s and were sent to an Arduino board (Mega 2560) equipped with a 16 bit analog to digital converter (Adafruit, ADS1115) and a real time clock module where the signal was collected and processed using custom software. For rate law experiments, all glassware, including the cuvette, were rinsed with ethanol and DI water, then dried with Ar (g). Gold solutions were prepared by varying ethanol concentration between 2.56 and 13.7 M (pure ethanol is 17.2 M) and varying the $Au^{III}Br_4^-$ concentration between 0.0125 and 1 mM, while maintaining 0.1 M HBr and 0.1 M $NaClO_4$. All experiments were conducted at room temperature (24 ± 1 °C). The solution's temperature did not change by more than 1 °C during the experiment.

2.2. Electrochemical reduction

For electrochemical experiments, a BASi EC Epsilon potentiostat was used along with a Pt gauze counter electrode and a Ag/AgBr (sat'd KBr) reference electrode. All electrochemical results are referred to using the polarographic rather than the IUPAC sign convention. The reference electrode was placed in a Luggin capillary. CPE experiments were performed using gold wire (25 μm diameter) as the working electrode, which was submerged ~1.0 cm into the solution. For each experiment, a new piece of gold wire was used. The solution used for CPE experiments contained 0.30 mM $Au^{III}Br_4^-$, 0.10 M $NaClO_4$, 0.10 M HBr in ethanol:water::1:1 (v/v). This solution was either (a) used as is, or prior to the CPE, (b) exposed to a 405 nm laser at 75 mW for 10 min, or (c) 1.0 mol equivalent of ascorbic acid (AA) was added. Both laser exposure and AA were used to reduce $Au^{III}Br_4^-$ to $Au^{I}Br_2^-$. Following CPE at different voltages, the working electrodes were rinsed, dried, and imaged by a scanning electron microscope (SEM) (Tescan MIRA 3).

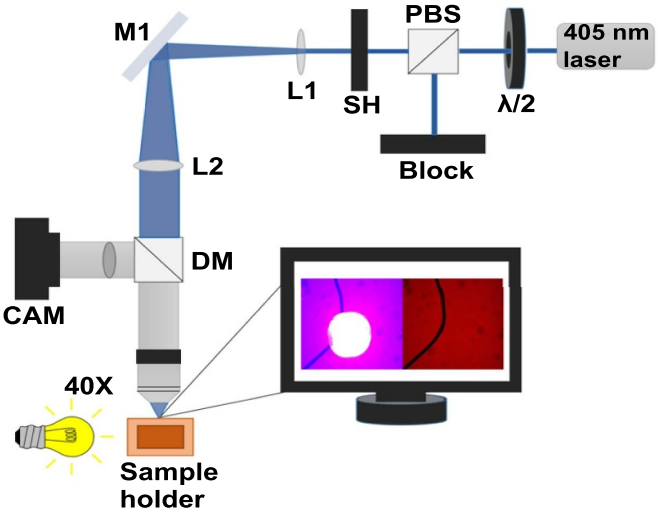

Figure 3. μPLATE laser schematic. The laser beam passes through a half-wave plate, a PBS, a shutter (SH), is expanded with lens (L1), and columnated with second lens (L2). A dichroic mirror (DM) transmits the laser beam and reflects illumination light from the sample into the camera (CAM). The laser passes through a 40× objective lens and onto the gold wire in the solution.

For QCM experiments, the working electrode was a 1.0 cm diameter gold film on a quartz wafer (SRS, QCM 25) which was connected to a QCM200 (SRS). The QCM was calibrated using a solution of 0.05 M $AgNO_3$ in 0.50 M HNO_3 per the manufacturer's instructions. The gold solution was 50 ml of 3 mM $Au^{III}Br_4^-$, 0.10 M $NaClO_4$, 0.10 M HBr in ethanol:water::1:1 (v/v). A solution of 0.015 M AA was added to the gold solution in five 20 μl aliquots, while a potential of +0.650 V vs Ag/AgBr was applied to the working electrode and the resonant frequency of the QCM was recorded.

To demonstrate the μPLATE concept, a custom sample holder was 3D printed which contained a slot for a window. The window was a 25 × 25 mm #1 coverslip. As shown in figure 3, a 40 × 0.75 NA objective lens was used to focus the 405 nm laser onto the gold wire which was submerged in the solution containing 13.1 mM $Au^{III}Br_4^-$, 0.1 M $NaClO_4$, 0.1 M HBr in ethanol:water::1:1. The lens in front of the camera was adjusted to be confocal with the laser such that both the image and the laser focused to the same plane. A CH Instruments potentiostat (CHI604E) was used to apply +0.550 V vs Ag/AgBr and a Pt gauze was used as the counter electrode. The potential was applied for 15 min, while the laser was focused onto the wire with 100 mW of power at the sample.

3. Results and discussion

3.1. Photochemical reduction of $Au^{III}Br_4^-$

The first step of the μPLATE method is the photochemical reduction of $Au^{III}Br_4^-$ to $Au^{I}Br_2^-$ via 405 nm light. This

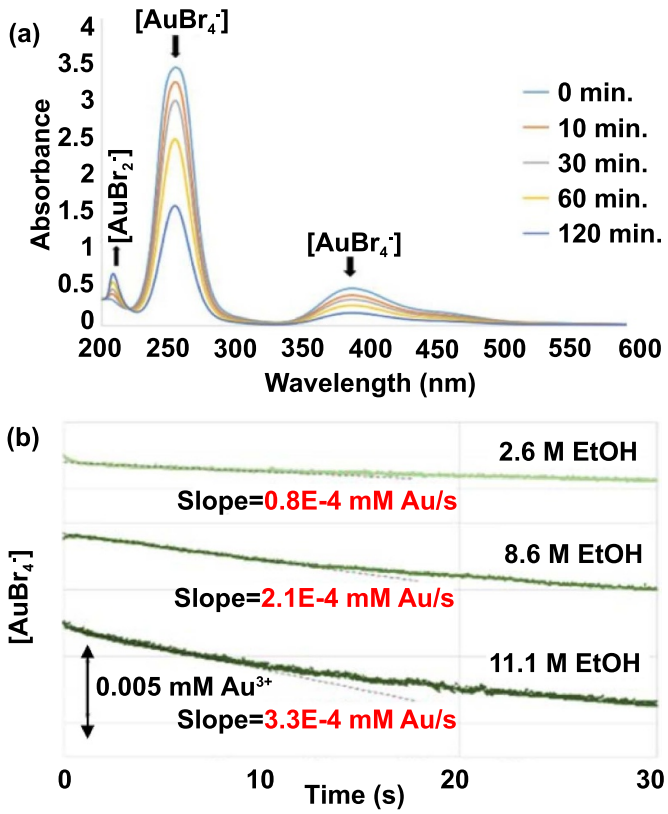

Figure 4. (a) Absorbance spectra of $Au^{III}Br_4^-$ and $Au^{I}Br_2^-$ over time upon 405 nm laser irradiation. (b) Photokinetics traces of $Au^{III}Br_4^-$ reduction at fixed initial $[Au^{III}Br_4^-] = 0.15$ mM and varied concentrations of ethanol with slopes fit to the first 10 s.

photoreductive elimination was first reported by Vogler and coworkers [35, 36] in ethanol, with the reaction:

$$AuBr_4^- + CH_3CH_2OH \rightarrow AuBr_2^- + CH_3CHO + 2\,HBr. \quad (3)$$

Figure 4(a) shows the absorption spectra of 0.15 mM $Au^{III}Br_4^-$ in ethanol:water::3:1 (v/v) as a function of time during exposure to a 405 nm laser. The 405 nm laser was chosen because it overlaps sufficiently with the $Au(III)Br_4^-$ peak centered at 395 nm but is not absorbed by $Au(I)Br_2^-$, which has a peak absorbance at 210 nm. As the time of exposure increases, the amount of $Au^{III}Br_4^-$ in the solution decreases while the presence of $Au^{I}Br_2^-$ increases, showing the direct relationship between the disappearance of $Au^{III}Br_4^-$ and the appearance of $Au^{I}Br_2^-$. Notably, there is no peak present corresponding to the absorption due to colloidal gold (~520 nm), indicating that while 405 nm light will reduce $Au^{III}Br_4^-$, there is no further reduction of $Au^{I}Br_2^-$ to colloidal gold [37, 38]. This is important for the μPLATE technique, as it ensures that the only species present in the electroplating process are $Au^{III}Br_4^-$ and $Au^{I}Br_2^-$.

To understand the kinetics of this photoreduction better, we used the method of initial rates, varying the concentration of ethanol and $Au^{III}Br_4^-$ as well as the power of the laser. The concentration of $Au^{III}Br_4^-$ over time is plotted (figure 4(b)) and the slope is equal to the rate of disappearance (mM Au s^{-1}) which is measured during the first 10 s of exposure. Table 1 shows data from nine trials, a subset of the 100+ trials that were used to determine the rate law of the reaction.

To convert the change in absorbance to concentration, the extinction coefficient of $Au^{III}Br_4^-$ at 405 nm was used. This value was determined from a Beer–Lambert plot to be 3.58 mM^{-1} cm^{-1} (data not shown). Over the concentration range tested, the rate constant, k, was determined to be 7 ($\pm$3) $\times$ 10^{-6} $mM^{2/3}$ M^{-1} mW^{-1}, and the rate law is shown in (4):

$$\text{Rate} = k\left[Au^{III}Br_4^-\right]^{\frac{1}{3}}[EtOH]^1 p^1. \quad (4)$$

3.2. *Electrochemistry of $Au^{III}Br_4^-$ and $Au^{I}Br_2^-$*

The second step of the μPLATE technique selectively plates $Au^{I}Br_2^-$ created via irradiation by 405 nm light. This step hinges on $Au^{III}Br_4^-$ plating at a more positive potential than $Au^{I}Br_2^-$, thus ensuring that only $Au^{I}Br_2^-$ is deposited onto the surface of the metal. The plating bath consists of $NaClO_4$, which acts as a supporting electrolyte, $Au^{III}Br_4^-$, which acts as a source of $Au^{I}Br_2^-$, and HBr, which solubilizes $Au^{I}Br_2^-$. The ethanol is added to act as a photochemical reducing agent as shown in equation (3).

For these experiments, gold was plated onto a gold wire. The gold wire was selected because of its convenience of preparation, both for the μPLATE procedure and because it can be easily imaged by optical and electron microscopy. Materials besides gold can be used, but may require an overpotential to initiate deposition, which could change as the surface becomes coated. For this proof of principle work we wanted to maintain a constant applied potential throughout the entire deposition and so chose to deposit gold on gold.

Figure 5 shows a series of SEM images of gold wires in which electrodeposition by CPE was attempted under varying conditions. In the left column, the wires were placed in a solution that contained only $Au^{III}Br_4^-$. In the middle column, the wires were placed in a solution of $Au^{III}Br_4^-$ that had been exposed to a 405 nm laser to generate $Au^{I}Br_2^-$, resulting in a mixture of both $Au^{I}Br_2^-$ and $Au^{III}Br_4^-$. In the right column, AA was added to a solution of $Au^{III}Br_4^-$ to convert all $Au^{III}Br_4^-$ to $Au^{I}Br_2^-$ [39]. The AA was used as a control as a means of chemically generating $Au^{I}Br_2^-$ independent of photoreduction to test the selectivity of electrodeposition. All sets of wires were held at varying potentials for 10 min and then imaged by a SEM. The images show there exists a voltage threshold near +0.500 V, (vs Ag/AgBr) above which the $Au^{III}Br_4^-$ does not reduce; however, at this same voltage and even at +0.600 V $Au^{I}Br_2^-$ readily plates. In the solution containing a mixture of $Au^{III}Br_4^-$ and photoreduced $Au^{I}Br_2^-$, some deposition can be seen at +0.500 V and less so at +0.600 V. From these results we conclude that $Au^{I}Br_2^-$ can be selectively deposited from a mixture of $Au^{I}Br_2^-$ and $Au^{III}Br_4^-$.

We also performed CPE experiments with a QCM to gain a better understanding of the kinetics of the selective

Table 1. Kinetics data from nine trials of over 100 trials.

[Au] (mM)	[EtOH] (M)	Power (mW)	Rate (10^{-4} mM Au s^{-1})	Rate constant, k (10^{-5} $mm^{2/3}$ M^{-1} mW^{-1})
0.05	8.6	8.0	1.5	6.1
0.30	8.6	8.0	3.0	6.6
1.00	8.6	8.0	4.2	6.1
0.15	2.6	8.0	0.8	7.4
0.15	8.6	8.0	2.1	5.8
0.15	11.1	8.0	3.3	6.9
0.15	8.6	2.0	0.8	8.4
0.15	8.6	4.0	1.2	6.5
0.15	8.6	6.0	3.3	5.8

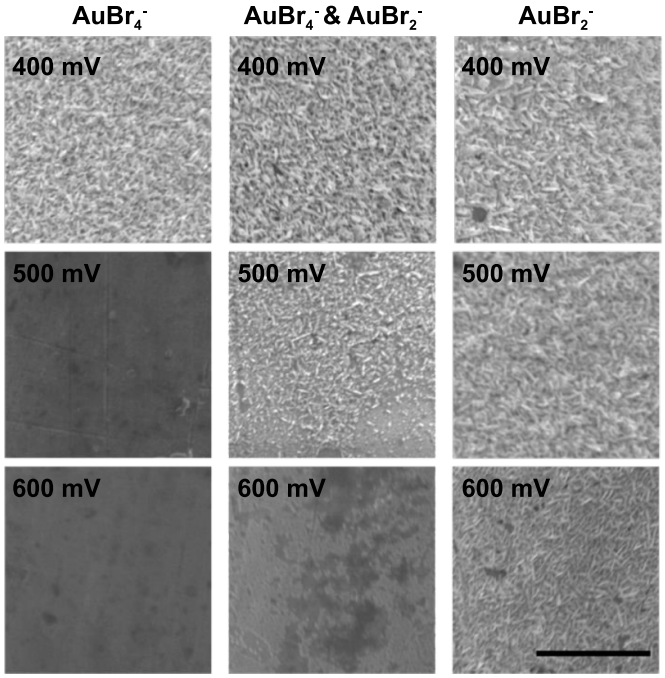

Figure 5. SEM images of electrodeposition in a potential window of +0.400–0.600 V (vs Ag/AgBr) on gold wires from solutions of $Au^{III}Br_4^-$ (left column), a photoreduced mixture of $Au^{III}Br_4^-$ and $Au^{I}Br_2^-$ (middle column), and $Au^{I}Br_2^-$ (right column). The left column shows electrodeposition of $Au^{III}Br_4^-$ at +0.400 V only, the middle column shows electrodeposition of $Au^{I}Br_2^-$ at +0.400 and +0.500 V, and a small amount at +0.600 V, and the right column shows electrodeposition of $Au^{I}Br_2^-$ at +0.400, +0.500, and +0.600 V. Scale bar is 5 μm.

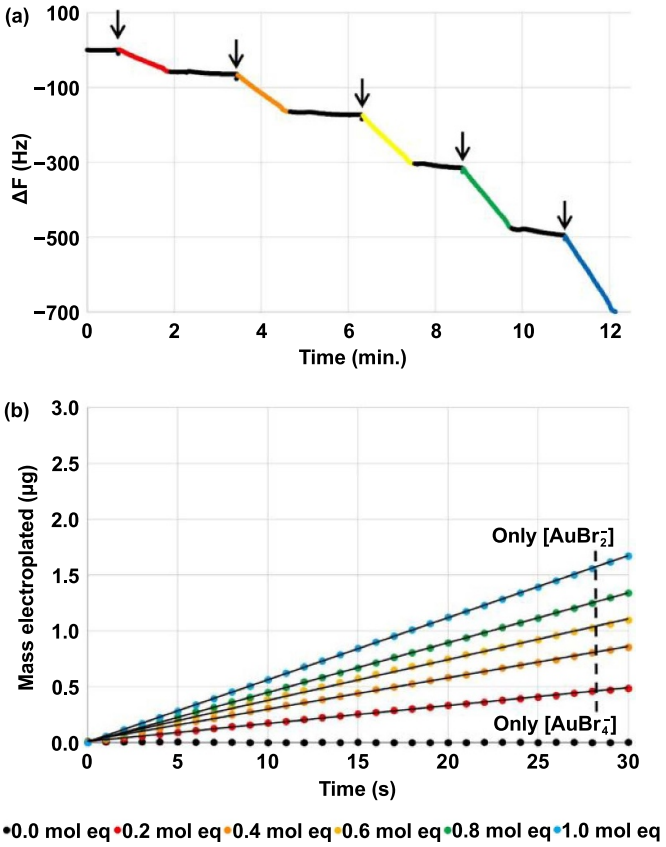

Figure 6. QCM electrodeposition in a solution containing $Au^{III}Br_4^-$ as it is converted to $Au^{I}Br_2^-$. (a) The change in resonance frequency was measured by the QCM during the titration with the arrows indicating when additions of AA occurred. (b) The additional mass of gold deposited in the first 30 s after each injection of AA is shown.

electrodeposition of $Au^{I}Br_2^-$ and $Au^{III}Br_4^-$. For this experiment, a calibrated gold QCM electrode was placed in a solution containing 0.15 mmol of $Au^{III}Br_4^-$. Next, 200 μl of 0.15 M AA was titrated into the $Au^{III}Br_4^-$ solution and a CPE experiment was performed, holding the voltage at +0.650 V (vs Ag/AgBr) while monitoring the QCM resonant frequency. As shown in figure 6(a) the decreasing frequency corresponds to the electrodeposition of $Au^{I}Br_2^-$. After 1 min the applied voltage was turned off and the QCM was allowed to stabilize for ∼1 min before the process was repeated. Five additions of AA were performed which converted all $Au^{III}Br_4^-$ to $Au^{I}Br_2^-$. The figure 6(a) shows the QCM trace over the course of the experiment, with arrows indicating when the AA was added. The QCM data for the first 30 s following each addition are replotted in figure 6(b) after converting the change in resonance frequency to mass. The slopes of the QCM data increase with more AA, indicating that higher concentrations of $Au^{I}Br_2^-$ result in higher rates of plating.

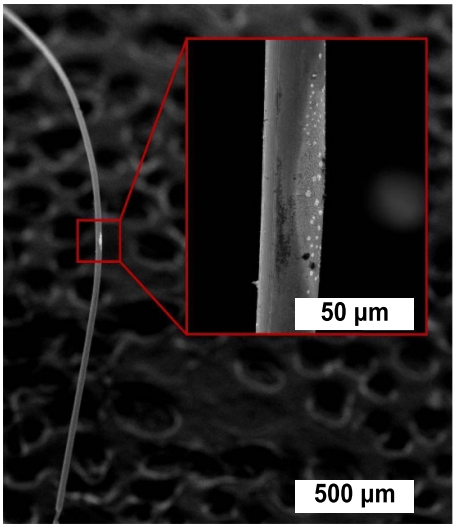

Figure 7. SEM images showing selective deposition of $Au^{I}Br_2^-$ onto the gold wire electrode which was held at a potential of +0.550 V while being exposed to a 405 nm laser.

These data further substantiate that, within the potential window, $Au^{I}Br_2^-$ will selectively plate in a solution where both $Au^{III}Br_4^-$ and $Au^{I}Br_2^-$ are present.

3.3. *Application of μPLATE*

A proof of principle experiment was performed using the experimental setup shown in figure 3. A gold wire was placed in a solution of $Au^{III}Br_4^-$, and it was exposed to a focused laser while a potential of +0.550 V (vs Ag/AgBr) was applied. This potential does not reduce $Au^{III}Br_4^-$ but can selectively reduce $Au^{I}Br_2^-$. Following the 15 min exposure, the sample was rinsed and imaged by a SEM. Figure 7 shows that gold was locally deposited at a spot on the wire over an approximately 100 μm long patch. The deposited gold is on the order of 1 μm thick and has granular flakes, similar to those shown in figure 5, with grain sizes of ∼100 nm. We believe the deposition took place by the two steps involved in μPLATE because during the exposure we did not see any evidence of a photothermal process taking place. That is, no bubbles or convective currents were observed near the focal point of the laser, which agrees with the kinetics trials where the temperature was observed to have not changed during the laser exposure.

Using the rate law equation (4), the electron micrograph in figure 7, and the CPE data, we can estimate the overall efficiency of the μPLATE process and its rate-limiting step. The amount of gold deposited in figure 7 is ∼1000 μm^3 (100 × 10 × 1 μm), which corresponds to ∼0.1 nmoles of gold. The rate law equation applied over the focal cone of light in the sample is estimated to generate ∼15 $\mu M\ s^{-1}$ of $Au^{I}Br_2^-$, which totals ∼0.1 nmoles over a 15 min period. Thus it would seem that the amount of $Au^{I}Br_2^-$ generated is approximately equal to the amount of Au^0 plated. Therefore, the efficiency of the μPLATE process, to a zeroth order approximation, is >10%. Given that the amount of gold electrodeposited is comparable to the amount estimated to have been photoreduced, we believe the rate limiting step is the first step, which is the photoreduction of $Au^{III}Br_4^-$. The CPE data for the second step, which is electrodeposition, indicate a higher rate of electrodeposition compared to photoreduction, but we believe a significant fraction of this current is non-Faradaic, since it is not possible to deposit $Au^{I}Br_2^-$ faster than it is created. It is hard to know exactly what the Faradaic current due solely to electrodeposition is, but the total CPE current implies that it is at least as fast as the rate-limiting photoreduction step.

While the μPLATE method has been demonstrated as we hypothesized, further optimization is necessary. The diffraction limited laser focal spot should be ∼0.5 μm in diameter but the deposition area is significantly larger. We believe this is because the locally generated $Au^{I}Br_2^-$ is free to diffuse in the solution before being plated. Also, the rate of deposition is likely made slower by this diffusion process.

4. Conclusion

In conclusion, the μPLATE method is a novel approach for localized gold deposition. Within a potential window of +0.500 to +0.650 V (vs Ag/AgBr), $Au^{I}Br_2^-$ produced by photoreduction of $Au^{III}Br_4^-$ is selectively deposited onto a gold working electrode, resulting in localized plating. Although more work needs to be done to improve the speed and resolution of the μPLATE technique, we have shown that gold can be locally photoreduced and electroplated in a hybrid DLW-electrochemical patterning method.

Acknowledgments

The Bard Research Fund, the Bard Summer Research Institute, and the Sherman Fairchild Foundation are acknowledged for financial support. We also thank Prof. O Simoska for her assistance in preparing the mansuscript.

ORCID iDs

Stella Rose Schneeberg https://orcid.org/0000-0003-0005-9494
Christopher N LaFratta https://orcid.org/0000-0003-4585-6278

References

[1] Kohl P 2014 Electrodeposition of Gold *Modern Electroplating* 5th edn Schlesinger M and Paunovic M The ECS Series of Texts and Monographs (Hoboken, NJ: John Wiley & Sons Inc.) pp 115–31
[2] Sage A T, Besant J D, Lam B, Sargent E H and Kelley S O 2014 Ultrasensitive electrochemical biomolecular detection using nanostructured microelectrodes *Acc. Chem. Res.* **47** 2417–25
[3] Madou M J 2011 *Fundamentals of Microfabrication and Nanotechnology, Three-Volume Set* 3rd edn (Boca Raton, FL: CRC Press)

[4] Zhao C, Zhong G W, Kim D E, Liu J X and Liu X Y 2014 A portable lab-on-a-chip system for gold-nanoparticle-based colorimetric detection of metal ions in water *Biomicrofluidics* **8** 052107

[5] Grabill C N, Freppon D, Hettinger M and Kuebler S M 2019 Nanoscale morphology of electrolessly deposited silver metal *Appl. Surf. Sci.* **466** 230–43

[6] Tal A, Chen Y S, Williams H E, Rumpf R C and Kuebler S M 2007 Fabrication and characterization of three-dimensional copper metallodielectric photonic crystals *Opt. Express* **15** 18283–93

[7] Clukay C J, Grabill C N, Hettinger M A, Dutta A, Freppon D J, Robledo A, Heinrich H, Bhattacharya A and Kuebler S M 2014 Controlling formation of gold nanoparticles generated *in situ* at a polymeric surface *Appl. Surf. Sci.* **292** 128–36

[8] Formanek F, Takeyasu N, Tanaka T, Chiyoda K, Ishikawa A and Kawata S 2006 Selective electroless plating to fabricate complex three-dimensional metallic micro/nanostructures *Appl. Phys. Lett.* **88** 083110

[9] LaFratta C N 2016 Nanoreplication printing and nanosurface processing *Multiphoton Lithography: Techniques, Materials and Applications* ed J Stampfl, R Liska and A Ovsianikov (Weinheim: Wiley) pp 335–53

[10] Farrer R A, LaFratta C N, Li L J, Praino J, Naughton M J, Saleh B E A, Teich M C and Fourkas J T 2006 Selective functionalization of 3D polymer microstructures *J. Am. Chem. Soc.* **128** 1796–7

[11] Dupuy C G, Beach D B, Hurst Jr J E and Jasinski J M 1989 Laser induced deposition of copper from (triethylphosphine)cyclopentadienylcopper(I) *Chem. Mater.* **1** 16–18

[12] Jiang H Q, Jin S Y, Wang C, Ma R Q, Song Y Y, Gao M Y, Liu X T, Shen A G, Cheng G J and Deng H X 2019 Nanoscale laser metallurgy and patterning in air using MOFs *J. Am. Chem. Soc.* **141** 5481–9

[13] Uwada T, Wang S F, Liu T H and Masuhara H 2017 Preparation and micropatterning of gold nanoparticles by femtosecond laser-induced optical breakdown *J. Photochem. Photobiol.* A **346** 177–86

[14] Blasco E, Müller J, Müller P, Trouillet V, Schön M, Scherer T, Barner-Kowollik C and Wegener M 2016 Fabrication of conductive 3D gold-containing microstructures via direct laser writing *Adv. Mater.* **28** 3592–5

[15] Harada M and Kizaki S 2016 Formation mechanism of gold nanoparticles synthesized by photoreduction in aqueous ethanol solutions of polymers using *in situ* quick scanning x-ray absorption fine structure and small-angle x-ray scattering *Cryst. Growth Des.* **16** 1200–12

[16] LaFratta C N, Lim D, O'Malley K, Baldacchini T and Fourkas J T 2006 Direct laser patterning of conductive wires on three-dimensional polymeric microstructures *Chem. Mater.* **18** 2038–42

[17] Maruo S and Saeki T 2008 Femtosecond laser direct writing of metallic microstructures by photoreduction of silver nitrate in a polymer matrix *Opt. Express* **16** 1174–9

[18] Komori T, Furukawa T, Iijima M and Maruo S 2020 Multi-scale laser direct writing of conductive metal microstructures using a 405 nm blue laser *Opt. Express* **28** 8363–70

[19] Baldacchini T, Pons A C, Pons J, LaFratta C N, Fourkas J T, Sun Y and Naughton M J 2005 Multiphoton laser direct writing of two-dimensional silver structures *Opt. Express* **13** 1275–80

[20] Tanaka T, Ishikawa A and Kawata S 2006 Two-photon-induced reduction of metal ions for fabricating three-dimensional electrically conductive metallic microstructure *Appl. Phys. Lett.* **88** 081107

[21] Kaneko K, Sun H B, Duan X M and Kawata S 2003 Two-photon photoreduction of metallic nanoparticle gratings in a polymer matrix *Appl. Phys. Lett.* **83** 1426–8

[22] Wee L M and Li L 2005 Multiple-layer laser direct writing metal deposition in electrolyte solution *Appl. Surf. Sci.* **247** 285–93

[23] von Gutfeld R J and Sheppard K G 1998 Electrochemical microfabrication by laser-enhanced photothermal processes *IBM J. Res. Dev.* **42** 639–53

[24] von Gutfeld R J, Gallaway J W and West A C 2009 *In situ* immersion plating of copper and nickel on aluminum using laser pulses for oxide removal *J. Electrochem. Soc.* **156** D564–9

[25] Takai T, Nakao H and Iwata F 2014 Three-dimensional microfabrication using local electrophoresis deposition and a laser trapping technique *Opt. Express* **22** 28109–17

[26] Iwata F, Kaji M, Suzuki A, Ito S and Nakao H 2009 Local electrophoresis deposition of nanomaterials assisted by a laser trapping technique *Nanotechnology* **20** 235303

[27] Pan H, Hwang D J, Ko S H, Clem T A, Fréchet J M J, Bäuerle D and Grigoropoulos C P 2010 High-throughput near-field optical nanoprocessing of solution-deposited nanoparticles *Small* **6** 1812–21

[28] Ko S H, Pan H, Grigoropoulos C P, Luscombe C K, Fréchet J M J and Poulikakos D 2007 All-inkjet-printed flexible electronics fabrication on a polymer substrate by low-temperature high-resolution selective laser sintering of metal nanoparticles *Nanotechnology* **18** 345202

[29] Ko S H, Pan H, Grigoropoulos C P, Luscombe C K, Fréchet J M J and Poulikakos D 2007 Air stable high resolution organic transistors by selective laser sintering of ink-jet printed metal nanoparticles *Appl. Phys. Lett.* **90** 141103

[30] Chung J, Ko S, Bieri N R, Grigoropoulos C P and Poulikakos D 2004 Conductor microstructures by laser curing of printed gold nanoparticle ink *Appl. Phys. Lett.* **84** 801–3

[31] Chung J, Bieri N R, Ko S, Grigoropoulos C P and Poulikakos D 2004 In-tandem deposition and sintering of printed gold nanoparticle inks induced by continuous Gaussian laser irradiation *Appl. Phys.* A **79** 1259–61

[32] Xia K W *et al* 2020 Photo-induced electrodeposition of metallic nanostructures on graphene *Nanoscale* **12** 11063–9

[33] Liu S S, Yuan T L, Wei W, Su H and Wang W 2019 Photoassisted electrochemical micropatterning of gold film *Anal. Chem.* **91** 9413–8

[34] Evans D H and Lingane J J 1963 Standard potentials of the couples involving AuBr4−, AuBr2− and Au In bromide media *J. Electroanal. Chem.* **6** 1–10

[35] Vogler A and Kunkely H 2001 Photoreactivity of gold complexes *Coord. Chem. Rev.* **219–221** 489–507

[36] Kunkely H and Vogler A 1992 Photooxidation of $AuCl_2^-$ and $AuBr_2^-$ induced by ds excitation *Inorg. Chem.* **31** 4539–41

[37] Eustis S and El-Sayed M A 2006 Molecular mechanism of the photochemical generation of gold nanoparticles in ethylene glycol: support for the disproportionation mechanism *J. Phys. Chem.* B **110** 14014–9

[38] Eustis S, Hsu H Y and El-Sayed M A 2005 Gold nanoparticle formation from photochemical reduction of Au^{3+} by continuous excitation in colloidal solutions. A proposed molecular mechanism *J. Phys. Chem.* B **109** 4811–5

[39] Bai T T, Tan Y B, Zou J M, Nie M X, Guo Z R, Lu X and Gu N 2015 $AuBr_2^-$engaged galvanic replacement for citrate-capped Au-Ag alloy nanostructures and their solution-based surface-enhanced Raman scattering activity *J. Phys. Chem.* C **119** 28597–604